Cross section of $^{36}S(n,\gamma)^{37}S$

H. Beer
Forschungszentrum Karlsruhe, Institut für Kernphysik, P.O. Box 3640, D-76021 Karlsruhe, Germany

P. V. Sedyshev and Yu. P. Popov
Frank Laboratory of Neutron Physics, JINR, 141980 Dubna, Moscow Region, Russia

W. Balogh, H. Herndl, and H. Oberhummer
Institut für Kernphysik, Wiedner Hauptstrasse 8-10, TU Wien, A-1040 Vienna, Austria
(Received 18 July 1995)

At the Karlsruhe pulsed 3.75 MV Van de Graaff accelerator the $^{36}S(n,\gamma)^{37}S(5.05\ min)$ cross section was measured by the fast cyclic activation technique via the 3.103 MeV γ-ray line of the ^{37}S decay. Samples of elemental sulfur enriched in ^{36}S by 5.933% were irradiated between two gold foils which served as capture standards. The capture cross section was measured at neutron energies 25, 151, 176, and 218 keV, respectively. The $^{36}S(n,\gamma)^{37}S$ cross section in the thermonuclear and thermal energy range has been calculated using the direct-capture (DC) model combined with the folding procedure used for the determination of the potentials. The nonresonant experimental data for this reaction can be reproduced excellently using this method. The input parameters of the DC calculation (masses, Q values, nuclear density distributions, spectroscopic factors, spin-parity assignments, and excitation energies of the low-lying states of the residual nucleus) have been taken from the available experimental data.

PACS number(s): 25.40.Lw, 24.50.+g, 27.30.+t, 95.30.Cq

I. INTRODUCTION

In the past years the importance of the direct-reaction (DI) mechanism in nucleosynthesis has been realized. The DI dominates over the compound-nucleus (CN) reaction mechanism if there exist no CN levels near the threshold that can be excited in the reaction. For instance, this can be the case in reactions involving light nuclei, in the big-bang scenario as well as in stellar hydrogen and helium burning. Direct capture (DC) can also be of importance in proton capture by proton-rich target nuclei [1–6] in the rp process occurring in novas or x-ray bursts and in neutron capture by neutron-rich nuclei [7–11] in the inhomogenous big bang as well as in the s process taking place in helium burning of red giants. Furthermore, DC can dominate for neutron capture by light [9] and heavy [12–16] target nuclei far from stability in the α process and r process occurring in supernovas of type II, respectively. The reaction rates of the neutron-rich S isotopes are of interest in the nucleosynthesis of nuclei in the s process in the S-Cl-Ar-Ca region [14,15], inhomogenous big-bang scenario [17,10], and in the α-rich freeze out of the neutron-rich hot neutrino bubble in supernovae of type II [18–21].

For the rare isotope ^{36}S a significant abundance contribution is expected from the s-process nucleosynthesis. For quantitative analyses the size of the destruction rate, i.e., the neutron capture rate, is of fundamental importance to estimate the magnitude of the ^{36}S abundance formed by the weak and main s-process components. Using the statistical model the ^{36}S capture cross section has been estimated to be 300 μb at 30 keV by Woosley *et al.* [22]. The present measurement, the first experimental investigation of this cross section, applies the fast cyclic activation technique [23] developed at the Karlsruhe 3.75 MV Van de Graaff accelerator.

We investigate the capture reaction $^{36}S(n,\gamma)^{37}S$ from thermal (25.3 meV) to thermonuclear (25–218 keV) projectile energies and compare the calculated cross sections in the DC model with the experimental data. In Secs. II and III the activation technique is described and the experimental results are given. In Sec. IV we introduce the methods used for calculating the direct-capture (DC) cross sections. In Sec. V the experimental and theoretical results for the neutron-capture cross section of ^{36}S are compared and discussed.

II. FAST CYCLIC ACTIVATION TECHNIQUE

The measurements have been carried out at the Karlsruhe pulsed 3.75 Van de Graaff accelerator. A common activation measurement is subdivided into two parts: (1) the irradiation of the sample, (2) the counting of the induced activity [24]. The cyclic activation method is the repetition of the irradiation and activity counting procedure many times to gain statistics. Especially for nuclei with half-lives of only minutes or seconds, in our case ^{37}S with a half-life of 5.05 min, a large number of irradiation and counting cycles is needed. The time constants for each cycle which are chosen shorter than the fluctuations of the neutron beam and comparable or shorter than the decay rate λ of the measured isotope are, the irradiation time t_b, the counting time t_c, the waiting time t_w (the time to switch from the irradiation to the counting phase), and the total time $T=t_b+t_w+t_c+t_w'$ (t_w' the time to switch from the counting to the irradiation phase). In the actual ^{36}S measurements the runs were partly carried out with $t_b=19.58$ s, $t_c=19.24$ s, $T=40$ s, partly with $t_b=49.58$ s, $t_c=49.24$ s, $T=100$ s. The waiting time is in both cases $t_w=0.42$ s.

TABLE I. Sample characteristics and decay properties of the product nuclei ^{37}S and ^{198}Au.

Isotope	Chemical form	Enrichment (%)	Reaction	$T_{1/2}$	E_γ (keV)	Intensity per decay (%)
^{36}S	Sulfur powder	5.933	$^{36}S(n,\gamma)^{37}S$	5.05 min	3103	94.0±0.6
^{197}Au	Metallic	100	$^{197}Au(n,\gamma)^{198}Au$	2.69 d	412	95.50±0.096

The accumulated number of counts from a total of n cycles, $C=\Sigma_{i=1}^{n}C_i$, where C_i, the counts after the ith cycle, are calculated for a chosen irradiation time, t_b, which is short enough compared with the fluctuations of the neutron flux with [23]

$$C=\epsilon_\gamma K_\gamma f_\gamma \lambda^{-1}[1-\exp(-\lambda t_c)] \times\exp(-\lambda t_w)\frac{1-\exp(-\lambda t_b)}{1-\exp(-\lambda T)} \times N\sigma[1-f_b\exp(-\lambda T)]\sum_{i=1}^{n}\Phi_i \quad (1)$$

with

$$f_b=\frac{\Sigma_{i=1}^{n}\Phi_i\exp[-(n-i)\lambda T]}{\Sigma_{i=1}^{n}\Phi_i}.$$

The following additional quantities have been defined: ϵ_γ, Ge efficiency; K_γ, γ-ray absorption; f_γ, γ-ray intensity per decay; N, the number of target nuclei; σ, the capture cross section; Φ_i, the neutron flux in the ith cycle. The quantity f_b is calculated from the registered flux history of a ^6Li glass monitor.

The efficiency determination of the 35% HPGe detector (2 keV resolution at 1.332 MeV) has been reported elsewhere [7]. The γ-ray absorption was calculated using tables published by Storm and Israel [25] and Veigele [26]. The half-lives and the γ-ray intensities per decay of ^{37}S and ^{198}Au are given in Table I.

The activities of nuclides with half-lives of several hours to days, i.e., the activity of ^{198}Au, can be also counted after the end of the cyclic activation consisting of n cycles using

$$C_n=\epsilon_\gamma K_\gamma f_\gamma \lambda^{-1}[1-\exp(-\lambda T_M)]\exp(-\lambda T_W) \times[1-\exp(-\lambda t_b)]N\sigma f_b\sum_{i=1}^{n}\Phi_i. \quad (2)$$

Here T_M is the measuring time of the Ge detector and T_W the time elapsed between the end of cyclic activation and beginning of the new data aquisition.

Equations (1) and (2), respectively, contain the unknown quantities σ and the total neutron flux $\Sigma_{i=1}^{n}\Phi_i$. Therefore, cross section ratios can be formed for different isotopes exposed to the same total neutron flux. This is the basis for the determination of the ^{36}S capture cross section relative to the well-known standard ^{197}Au capture cross section [27]. As the ^{36}S sample to be investigated is characterized by a finite thickness it is necessary to sandwich the sample by two comparatively thin gold foils for the determination of the effective neutron flux at sample position. The activities of these gold foils were counted also individually after termination of the cyclic activation. The effective count rate of gold was obtained from these individual rates as well as from the accumulated gold count rate during the cyclic activation run. Therefore, the effective neutron flux at sample position was determined in two ways by way of the gold activation according to Eqs. (1) and (2). Using Eq. (1) has the advantage that saturation effects in the gold activity for irradiations over several days are avoided [23].

III. EXPERIMENTAL ARRANGEMENTS AND RESULTS

In Fig. 1 a scheme of the experimental setup is shown. The kinematically collimated neutron beam is generated with the $^7Li(p,n)$ reaction near the reaction threshold (1.912 MeV proton energy) with thick ^7Li targets (30 μm) and corresponds to a Maxwellian neutron spectrum with a thermal neutron energy of $kT=25$ keV [23–27]. The neutron spectra at the neutron energies 151, 176, and 218 keV were generated using thin Li targets (2.5 μm). The required proton energy conditions and the neutron spectra integrated over the solid angle of the sample were determined in time-of-flight (TOF) measurements before the actual activation

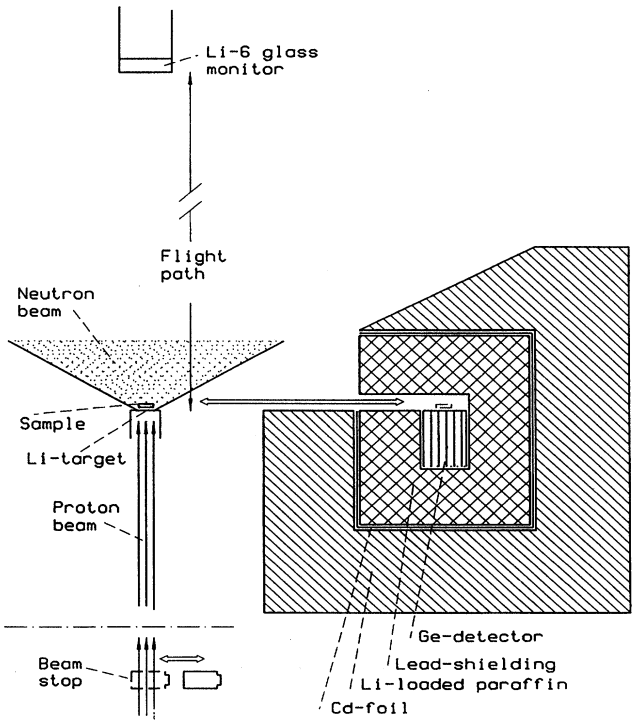

FIG. 1. Scheme of experimental setup.

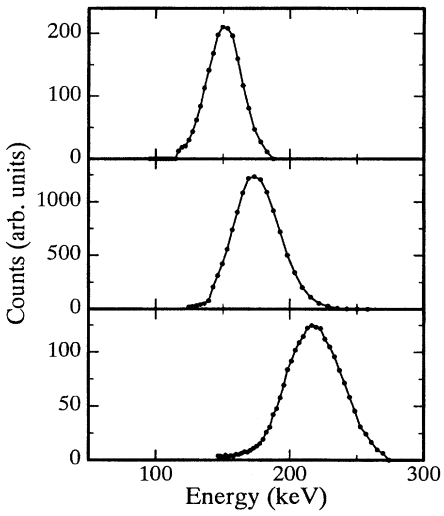

FIG. 2. Neutron spectra with mean neutron energies of 151 (top), 176 (middle), and 218 keV (bottom) at sample position. Using the proton energies and the metallic Li targets (2.5 μm thickness) of the actual activation measurements they were calculated from TOF spectra measured under different angles with respect to the beam axis.

runs using the accelerator in pulsed mode (Fig. 2). These neutron spectra are in good agreement with corresponding Monte Carlo calculations [28,29]. The proton beam was wobbled initiated by magnetic deflection to cover the area of the Li target. The beam profile formed was studied on a quartz target. To switch back and forth between sample irradiation and activity counting a fast sample changer operating with compressed air was used. Close to the beam line where the neutrons have been generated the Ge detector for activity counting, well shielded by lead and Li loaded paraffin, has been installed (Fig. 1). During the irradiation phase the analog to digital converter was gated to prevent data acquisition. The relative neutron flux was recorded continuously with a ^{6}Li glass detector. During the activity counting phase neutron generation was interrupted by a beam stop for the proton beam. This is essential to reduce all prompt accelerator dependent γ rays. The beam stop was installed in the beam line at the accelerator hall so that in the activity counting periods the experimental hall was free of prompt background radiation. In Table I the sample characteristics of ^{36}S and ^{197}Au and the decay properties of the product nuclei are listed. Table II gives a survey of the sample weights and the measured ^{36}S capture cross sections. The sulfur was pressed to self-supporting tablets of 6 mm diam, the gold foils on back and front side of the sulfur sample with regard to the impinging neutrons had the same dimensions. At 25 keV neutron energy measurements were carried out with sulfur sample masses between 20 and 100 mg. No significant effect from multiple neutron scattering was observed. A sample of the sulfur powder was also heated to 300 °C. No measurable weight loss due to absorbed water was found. In Fig. 3 the accumulated γ-ray intensity from one of the ^{36}S activations is shown. The γ line is well isolated on a low level of background counts.

The following systematic uncertainties were combined by quadratic error propagation: Au standard cross section, 1.5–3 %; Ge-detector efficiency, 6%; γ-ray intensity per decay, 0.6% for the ^{37}S and 0.1% for the ^{198}Au decay; divergence of neutron beam, 2-12 %; factor f_b, 1.5%; sample weight, <0.5%; and other systematic errors, 2%.

TABLE II. Sample weights and experimental ^{36}S capture cross sections.

Mean neutron energy (keV)	Mass of Au front side (mg)	Mass of sulfur (mg)	Mass of Au back side (mg)	Irradiation time (d)	σ (μb)	Uncertainty statistical (%)	Uncertainty total (%)
25	16.80	100.32	16.84	3.54	192	1.2	11.3
	16.61	95.32	16.64	1.70	195	1.1	10.5
	16.57	50.40	16.51	1.16	169	2.8	8.3
	16.57	50.40	16.51	1.70	168	2.3	8.1
	15.71	148.89	15.73	0.58	191	1.5	13.9
	8.86	50.11	8.80	2.70	178	1.0	8.3
	17.15	21.18	17.22	5.10	190	1.6	7.5
				Average	187±14		
151±15	16.38	94.96	16.71	3.70	85	3.3	9.5
	16.46	150.19	16.33	6.90	80	1.8	11.5
				Average	81±7		
176±20	17.35	94.94	17.34	2.40	114	7.2	11.4
	17.35	94.94	17.34	7.80	128	3.2	9.4
				Average	125±11		
218±23	17.39	150.00	17.39	3.20	87	6.3	11.2
	17.40	149.85	17.38	6.80	74	4.7	11.7
				Average	78±7		

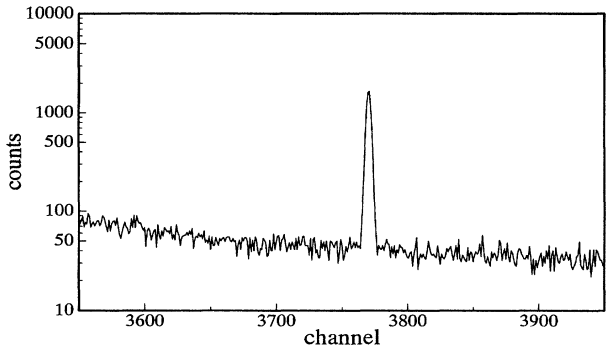

FIG. 3. Accumulated intensity of the 3103 keV ^{37}S γ line from the activation with a 100.32 mg sulfur sample.

IV. THEORETICAL ANALYSIS

A. Reaction mechanism and models

In nuclear reactions two extreme types of reaction mechanisms can exist: the compound-nucleus (CN) and the direct (DI) process. In the CN mechanism the projectile merges in the target nucleus and excites many degrees of freedom of the CN. The excitation proceeds by way of a multistep process and therefore has a reaction time typically of the order 10^{-16} s to 10^{-20} s. After this time the CN decays into various exit channels. The relative importance of the decay channels is determined by the branching ratios to the final states. In the DI process the projectile excites only a few degrees of freedom (e.g., single particle or collective). The excitation proceeds in one single step and has a characteristic time scale of 10^{-21} s to 10^{-22} s. This corresponds to the time it takes the projectile to pass through the target nucleus; this time is much shorter than the reaction time of CN processes.

B. Folding procedure

The folding procedure is used for calculating the nucleon-nucleus potentials to describe the elastic scattering data and the bound states. This method has been applied successfully in describing many nucleon-nucleus systems. In the folding approach the nuclear density ρ_A is folded with an energy and density dependent nucleon-nucleon interaction v_{eff} [30,31]

$$V(R)=\lambda V_F(R)=\lambda\int \rho_A(\vec{r})v_{\text{eff}}(E,\rho_A,|\vec{R}-\vec{r}|)d\vec{r} \quad (3)$$

with $\vec{R}$ being the separation of the centers of mass of the two colliding nuclei. The normalization factor λ is adjusted to reproduce the elastic scattering data the binding energies of the residual nuclei. The folding potentials of Eq. (3) were determined with the help of the code DFOLD [32].

C. Direct-capture model

In thermonuclear scenarios the projectile energy is well below the Coulomb and/or centrifugal barrier. Consequently, the CN formation may be suppressed, because there are almost no CN levels that can be populated, especially in light, magic, and far-off-stability nuclei. In this paper the theoretical cross sections are calculated by only considering the DC contributions. The theoretical cross section σ^{th} is obtained from the DC cross section σ^{DC} by [31,33]

$$\sigma^{\text{th}}=\sum_i C_i^2 S_i \sigma_i^{\text{DC}}. \quad (4)$$

The sum extends over the ground state and excited states in the final nuclei, where the spectroscopic factors S_i are known. The isospin Clebsch-Gordan coefficients are given by C_i. The DC cross sections σ_i^{DC} are essentially determined by the overlap of the scattering wave function in the entrance channel, the bound-state wave function in the exit channel and the multipole transition operator. The radial dependence of the wave functions in the DC integral is in our case determined uniquely by the folding potentials.

V. CALCULATIONS AND RESULTS

In the folding approach the nuclear density ρ_A for the stable nucleus ^{36}S was derived from the experimental charge distribution [34]. The normalization factor λ for $^{36}S(n,\gamma)^{37}S$ of the optical potential in the entrance channel was adjusted to fit the thermal ($^{36}S+n$)-scattering cross section of (1.1 ± 0.8) b [35]. Even so this cross section is not determined well, we fitted our normalization factor to reproduce 1.1 b. However, applying the same fitting procedure to the ($^{34}S+n$)-scattering cross section that is known much better [(1.52 ± 0.03) b [35]] we obtained almost the same volume integral per nucleon in the two cases ($^{34}S+n$: 501.7 MeV fm^3; $^{36}S+n$: 497.1 MeV fm^3). The imaginary part of the optical potential is small for the ($^{36}S+n$) channel and can be neglected. For the exit channels the normalization constants λ were adjusted to the energies of the ground and the excited states. The potentials obtained in this way ensure the correct behavior of the wave functions in the nuclear exterior.

The spectroscopic factors for one-nucleon stripping of ^{37}S were determined from the most recent experimental $^{36}S(d,p)^{37}S$ data [39]. We also carried out shell-model calculations using a combined sd and pf shell with an effective nucleon-nucleon interaction derived by Warburton *et al.* [36]. For these calculations the program OXBASH [37] was used to calculate the wave functions and spectroscopic factors. The calculated spectroscopic factors are larger than those extracted from the experimental $^{36}S(d,p)^{37}S$ data (see Table III). This fact might be due to the strong truncation of the model space (only one neutron in the pf shell for the negative parity states). Inclusion of more particle-hole excitations should give smaller spectroscopic factors. The masses and Q values for the transitions to the different states of the residual nucleus ^{37}S were taken from experimental data [38,39]. For the DC calculations the code TEDCA [41] was used.

The level scheme of the relevant levels for ^{37}S is shown in Fig. 4. The cross section for the reaction $^{36}S(n,\gamma)^{37}S$ obtained from the DC calculation is compared with the experimental data from the thermal to the thermonuclear energy region in Fig. 5. There are two types of $E1$ transitions contributing for the transitions to the residual nucleus ^{37}S. The first one comes from an s wave in the entrance channel exciting the negative-parity states $3/2^-$ and $1/2^-$ (see Table

TABLE III. Final states, Q values, transitions, and spectroscopic factors for the states of ^{37}S obtained from shell-model calculations and ^{36}S$(d,p)^{37}$S. Cross sections for ^{36}S$(n,\gamma)^{37}$S at 25.3 meV, 25 keV, 151 keV, 176 keV, and 218 keV using DC with the experimental data.

Final state	Q value [MeV]	Transition	Spectroscopic factor Shell model	Spectroscopic factor (d,p) reaction [39]	Cross section 25.3 meV [mb]	Cross section 25 keV [μb]	Cross section 151 keV [μb]	Cross section 176 keV [μb]	Cross section 218 keV [μb]
$\frac{7}{2}^-$	4.303	$d\rightarrow f$	0.91	0.50	0.0	0.0	0.1	0.2	0.2
$\frac{3}{2}^-$	3.657	$s\rightarrow p$	0.86	0.55	157.1	158.0	64.3	59.5	53.5
$\frac{3}{2}^+$	2.906	$p\rightarrow d$	0.07	0.03	0.0	0.0	0.0	0.0	0.0
$\frac{3}{2}^-$	2.312	$s\rightarrow p$	0.12	0.03	5.3	5.3	2.1	2.0	1.8
$\frac{1}{2}^-$	1.666	$s\rightarrow p$	0.97	0.47	28.3	28.5	11.6	10.8	9.7
			Total cross section: DC		190.7	191.8	78.1	72.5	65.2
			Total cross section: experiment		150±30 [a]	187±14	81±7	125±11	78±7

[a]Reference [35].

III). These transitions give the well-known $1/v$ behavior (see Fig. 4). The second type of $E1$ transition comes from an initial p wave and excites the positive-parity state $3/2^+$ in the final nucleus. This transition has a v behavior and can be neglected in the relevant energy range (see Fig. 4 and Table III). The $E1$ transition to the $7/2^-$ ground state of ^{37}S can also be neglected, because of the higher centrifugal barrier necessary for the incoming d wave (see Table III). As can be seen from Fig. 4 this contribution effects the deviation from an $1/v$ behavior of the cross section only above about 700 keV.

The spin and parity assignments of the final states in ^{37}S, the Q values for the transitions to the different final states, the spectroscopic factors obtained from ^{36}S$(d,p)^{37}$S and shell-model calculations are shown in Table III. Also in this table the calculated cross sections for ^{36}S$(n,\gamma)^{37}$S at 25.3 meV, 25, 151, 176, and 218 keV using DC with the spectroscopic factors obtained from the (d,p) data are compared with the experimental data.

We have determined the thermonuclear-reaction-rate factor $N_A\langle\sigma v\rangle$ [40]. Since the cross section follows a $1/v$ law up to 150 keV we obtain a constant reaction-rate factor

$$N_A\langle\sigma v\rangle = 2.56\times 10^4 \ \text{cm}^3\,\text{mole}^{-1}\,\text{s}^{-1}. \quad (5)$$

VI. DISCUSSION

Direct-capture calculations using the folding procedure can excellently reproduce the nonresonant experimental data for the capture cross section by the neutron-rich sulfur isotope ^{36}S in the thermal and thermonuclear energy region. The enhancement in the region of 176 keV comes from resonant contributions [39] not considered in the DC calculation.

DC is also the dominant reaction mechanism for neutron capture by neutron-rich isotopes far-off stability occurring in the α and r process. For such isotopes the Q value and

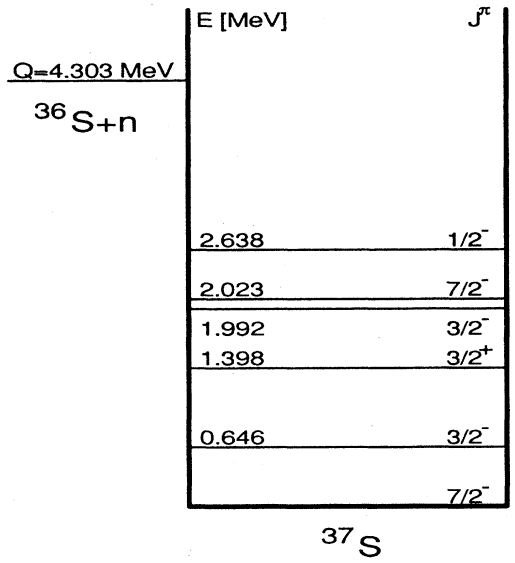

FIG. 4. Level scheme of ^{37}S.

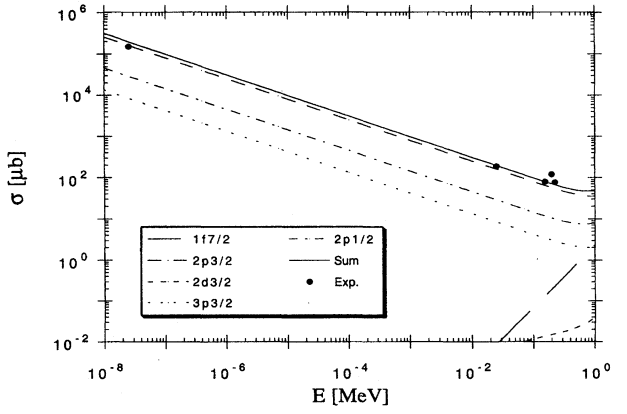

FIG. 5. Comparison of the DC cross section for ^{36}S$(n,\gamma)^{37}$S with the experimental data from thermal to thermonuclear projectile energies. The DC contributions for the different transitions to the final states of ^{37}S as well as the sum of all transitions (solid curve) is shown. The experimental data at the thermal energy have been taken from Ref. [35].

therefore the excitation energy of the compound nucleus gets still lower, leading to a further substantial diminution of the level density of the compound nucleus. Thus, the DC contribution becomes the dominating reaction mechanism. Nuclear-structure models are indispensable for extrapolating reaction rates to nuclei near and far-off the region of stability, because only a limited or no experimental information is available in this region. The DC cross reaction $^{36}S(n,\gamma)^{37}S$ can be considered as a benchmark of different nuclear-structure models (shell model, relativistic mean field theory, quasiparticle random phase approximation, Hartree-Fock-Bogoliubov theory) for calculating neutron-capture cross sections by neutron-rich nuclei taking place in the α or r process [42].

The s-process production of ^{36}S was recently discussed quantitatively by Schatz *et al.* [29] but without a reliable $^{36}S(n,\gamma)$ cross section. The s-process reaction network in the sulfur to calcium region contains (n,γ), (n,p), and (n,α) reactions. The ^{36}S production is mediated by the $^{36}Cl(n,p)^{36}S$ reaction from seed nuclei with mass numbers <36. But also seed nuclei >36 can contribute through the $^{39}Ar(n,\alpha)^{36}S$ reaction channel. Besides its formation the destruction of ^{36}S by the (n,γ) reaction is important. A decrease in the $^{36}S(n,\gamma)^{37}S$ cross section leads to a corresponding increase of the abundance formed. As our measured $^{36}S(n,\gamma)^{37}S$ value is by a factor of 1.8 smaller than the estimate of Woosley *et al.* [22] the s-process abundance production of ^{36}S will be enhanced by this factor. The quantitative analysis requires also model parameters for the main and especially the weak s-process component. This information can be obtained from the analysis of the s-process beyond $A=56$ [43].

Note added in proof. There is a discrepancy in the spectroscopic factors extracted from the experimental data of $^{36}S(d,p)^{37}S$ between the original work in G. Eckle *et al.*, Nucl. Phys. **A491**, 205 (1989), Table 1 and the compilation of P. M. Endt, Nucl. Phys. **A521**, 1 (1990), Table 37.4. The reason for this discrepancy is not clear (H. Clement and P. M. Endt, private communication). In this paper we used the values of P. M. Endt. If the values for the original work by G. Eckle *et al.* are employed, the values of the calculated theoretical total direct-capture cross sections for $^{36}S(n,\gamma)^{37}S$ given in this paper should be reduced by 20%.

ACKNOWLEDGMENTS

We would like to thank our technician G. Rupp and the Van de Graaff staff members, E.-P. Knaetsch, D. Roller, and W. Seith for their skill in preparing the metallic Li targets in the required quality. We are also indebted to the Van de Graaff staff for providing reliable beam conditions of the accelerator. We thank the Fonds zur Förderung der wissenschaftlichen Forschung in Österreich (Project No. S7307-AST) and the Östereichische Nationalbank (Project No. 5054) for their support. Two of the authors (H.H. and H.O.) express their gratitude to M. Wiescher for valuable and helpful discussions during their stay at the University of Notre Dame. One of the authors (H.B.) is grateful to Ch. Theis and S. Jaag for support in special problems of the computer system for data acquisition and handling.

[1] G. Hardie, R. E. Segel, A. J. Elwyn, and J. E. Monahan, Phys. Rev. C **38**, 2003 (1988).

[2] M. Wiescher and J. Görres, Astrophys. J. **346**, 1041 (1989).

[3] S. M. Graff, J. Görres, M. Wiescher, R. E. Azuma, J. King, J. Vise, G. G. Hardie, and T. R. Wang, Nucl. Phys. **A510**, 346 (1990).

[4] J. Görres, S. M. Graff, M. Wiescher, R. E. Azuma, C. A. Barnes, H. W. Becker, and T. R. Wang, Nucl. Phys. **A517**, 329 (1990).

[5] C. Iliadis, U. Giesen, J. Görres, M. Wiescher, S. Graff, R. E. Azuma, and C. A. Barnes, Nucl. Phys. **A539**, 97 (1992).

[6] H. Herndl, J. Görres, M. Wiescher, B. A. Brown, and L. Van Wormer, Phys. Rev. C **52**, 1078 (1995).

[7] H. Beer, M. Wiescher, F. Käppeler, J. Görres, and P. E. Koehler, Astrophys. J. **387**, 258 (1992).

[8] H. Beer, F. Käppeler, and M. Wiescher, in *Proceedings of the 8th International Symposium on Capture Gamma-Ray Spectroscopy and Related Topics,* Fribourg, Switzerland, 1994, edited by J. Kern (World Scientific, Singapore, 1994), p. 756.

[9] K. Grün, R. Pichler, and H. Oberhummer, in *Neutrons and Their Applications*, edited by G. Vourvopolous and T. Paradellis [Proc. SPIE **2339**, 77 (1995)].

[10] T. Rauscher, J. H. Applegate, J. C. Cowan, F.-K. Thielemann, and M. Wiescher, Astrophys. J. **429**, 499 (1994).

[11] J. Meißner, H. Schatz, H. Herndl, M. Wiescher, H. Beer, and F. Käppeler, in *Proceedings of Nuclei in The Cosmos III*, edited by M. Busso, R. Gallino, and C. M. Raiteri, AIP Conf. Proc. No. 327 (AIP, New York, 1995), p. 307.

[12] G. J. Mathews, A. Mengoni, F.-K. Thielemann, and W. A. Fowler, Astrophys. J. **270**, 740 (1983).

[13] W. Balogh, R. Bieber, H. Oberhummer, T. Rauscher, K.-L. Kratz, P. Mohr, G. Staudt, and M. M. Sharma, in *Proceedings of the European Workshop on Heavy Element Nucleosynthesis,* Budapest, 1994, edited by E. Somoraj and Zs. Fülöp (Institute of Nuclear Research of the Hung. Acad. of Sci., Debrecen, 1994), p. 67.

[14] H. Beer and R.-D. Penzhorn, Astron. Astrophys. **174**, 323 (1987).

[15] S. Druyts, C. Wagemans, and P. Geltenbort, Nucl. Phys. **A573**, 291 (1994).

[16] T. Rauscher, R. Bieber, S. Lingner, and H. Oberhummer, in *Proceedings of Nuclei in The Cosmos III* [11], p. 183.

[17] R. Malaney and G. J. Mathews, Phys. Rep. **229**, 145 (1993).

[18] S. E. Woosley and R. D. Hoffmann, Astrophys. J. **395**, 202 (1992).

[19] S. E. Woosley, J. R. Wilson, G. J. Mathews, R. D. Hoffmann, and B.S. Meyer, Astrophys. J. **433**, 229 (1994).

[20] W. M. Howard, S. Gloriely, M. Rayet, and M. Arnould, Astrophys. J. **417**, 713 (1993).

[21] J. Witti, H.-Th. Janka, and K. Takahashi, Astron. Astrophys. **286**, 841 (1994).

[22] S. E. Woosley, W. A. Fowler, J. A. Holmes, and B. A. Zimmer-

man, At. Data Nucl. Data Tables **22**, 371 (1978).
[23] H. Beer, G. Rupp, F. Voß, and F. Käppeler, Nucl. Instrum. Methods Phys. Res. Sect. A **337**, 492 (1994).
[24] H. Beer and F. Käppeler, Phys. Rev. C **21**, 53 (1980).
[25] E. Storm and H. Israel, Nucl. Data Tables A **7**, 565 (1970).
[26] WM. J. Veigele, At. Data Nucl. Data Tables **5**, 51 (1973).
[27] W. Ratynski and F. Käppeler, Phys. Rev. C **37**, 595 (1988).
[28] H. Schatz, Diplomarbeit, Universität Karlsruhe, 1992.
[29] H. Schatz, S. Jaag, G. Linker, R. Steininger, and F. Käppeler, Phys. Rev. C **51**, 379 (1995).
[30] A. M. Kobos, B. A. Brown, R. Lindsay, and G. R. Satchler, Nucl. Phys. **A425**, 205 (1984).
[31] H. Oberhummer and G. Staudt, in *Graduate Texts in Contemporary Physics, Nuclei in the Cosmos*, edited by H. Oberhummer (Springer Verlag, Heidelberg, 1991), p. 25.
[32] H. Abele, code DFOLD, Universität Tübingen, 1991 (unpublished).
[33] P. Mohr, H. Abele, R. Zwiebel, G. Staudt, H. Krauss, H. Oberhummer, A. Denker, J. W. Hammer, and G. Wolf, Phys. Rev. C **48**, 1420 (1993).
[34] H. De Vries, C. W. De Jager, and C. De Vries, At. Data Nucl. Data Tables **36**, 495 (1987).
[35] V. F. Sears, Neutron News **3**, 26 (1992).
[36] E. K. Warburton, J. A. Becker, D. J. Millener, and B. A. Brown, Brookhaven National Report No. 40890, 1987 (unpublished).
[37] B. A. Brown, A. Etchegoyen, W. D. M. Rae, and N.S. Godwin, code OXBASH, 1984 (unpublished).
[38] G. Audi and A. H. Wapstra, Nucl. Phys. **A565**, 1 (1993).
[39] P. M. Endt, Nucl. Phys. **A521**, 1 (1990).
[40] W. A. Fowler, G. R. Caughlan, and B. A. Zimmerman, Annu. Rev. Astron. Astrophys. **5**, 525 (1967).
[41] H. Krauss, code TEDCA, TU Wien, 1992 (unpublished).
[42] H. Oberhummer, W. Balogh, R. Bieber, H. Herndl, U. Langer, T. Rauscher, and H. Beer, in *Proceedings of the International Conference on Exotic Nuclei and Atomic Masses 1995 (ENAM95),* Arles, France (Les Editions Frontières, Gif-sur-Yvette, France, to be published).
[43] H. Beer, B. Spettel, H. Palme, in *Proceedings of Nuclei in The Cosmos III* [11], p. 307.